CANMET

REPORT 79-2

Canada Centre for Mineral and Energy Technology

Centre canadien de la technologie des minéraux et de l'énergie

SYNTHESIS AND CHARACTERIZATION OF ZIRCONIA ELECTROLYTES FOR POTENTIAL USE IN ENERGY CONVERSION SYSTEMS

T.A. WHEAT

MINERALS RESEARCH PROGRAM
MINERAL SCIENCES LABORATORIES

Energy, Mines and Resources Canada
Énergie, Mines et Ressources Canada

NOVEMBER 1978

Available in Canada through

Authorized Bookstore Agents
and other bookstores

or by mail from

Canadian Government Publishing Centre
Supply and Services Canada
Hull, Quebec, Canada K1A 0S9

CANMET
Energy, Mines and Resources Canada,
555 Booth St.,
Ottawa, Canada K1A 0G1

or through your bookseller.

Catalogue No. M38–13/79-2
ISBN 0-660-10405-9

Canada: $1.75
Other countries: $2.10

Price subject to change without notice.

En vente au Canada par l'entremise de nos

agents libraires agréés
et autres librairies

ou par la poste au:

Centre d'édition du gouvernement du Canada
Approvisionnements et Services Canada
Hull, Québec, Canada K1A 0S9

CANMET
Énergie, Mines et Resources Canada,
555, rue Booth
Ottawa, Canada K1A 0G1

ou chez votre libraire.

Nº de catalogue M38–14/79-2
ISBN 0-660-10405-9

Canada: $1.75
Hors Canada: $2.10

Prix sujet à changement sans avis préalable.

SYNTHESIS AND CHARACTERIZATION OF ZIRCONIA ELECTROLYTES FOR POTENTIAL USE IN ENERGY CONVERSION SYSTEMS

by

T.A. Wheat*

ABSTRACT

The present work is part of a program to develop ionically conducting materials for potential use in energy storage and conversion systems. With applications in high energy-density batteries, magneto-hydrodynamic (MHD) generators, fuel cells and sensors, they are playing an increasingly important role in developing more efficient energy storage and conversion devices.

Of more than 30 presently known solid-state ionically conducting materials, zirconia is probably the most extensively used. It combines the desirable properties of refractoriness, high mechanical strength and electrical conductivity, making it a candidate material for use in both fuel cells and MHD generators. Because of limited data available in the literature, particularly on its microstructural, electrical and thermal properties as a function of thermal history, a study was initiated to determine the stability of various compositions in the $CaO-ZrO_2$ system appropriate to fuel cell and MHD applications.

Using a wet-chemical procedure, a series of compositions having between 0 and 22.2 mol % CaO, was prepared and subsequently formed into sintered samples having a relative density from 95 to 98%. Sintered samples were prepared of each composition with a geometry appropriate for determining the thermal, electrical or microstructural characteristics. This report covers only the microstructural aspects of powder synthesis and the development of sintered materials.

Using the reactive, homogeneous, chemically prepared powders, it has been shown that cubic and monoclinic zirconia can coexist in compositions containing up to 10 mol % CaO. From 10 to 20 mol % CaO, only the cubic phase is formed, whereas at higher CaO concentrations the cubic phase coexists with $CaZrO_3$. The change from a two-phase to single-phase system as the CaO concentration is increased above 10 mol %, increases the grain size nearly an order of magnitude.

---

*Research Scientist, Ceramic Section, Industrial Minerals Laboratory, Mineral Sciences Laboratories, CANMET, Energy, Mines and Resources Canada, Ottawa.

It has been found that 5 and 7.6 mol % CaO materials develop considerable stress during the cooling stage of the firing cycle. As a result, they undergo a progressive and irreversible expansion with each thermal shock cycle: the magnitude of the expansion is proportional to the severity of the thermal shock. The microstructural texture of these partially stabilized materials was also shown to be dependent on the thermal history and hence a strong dependence of the electrical and thermal properties can be anticipated.

SYNTHESE ET CARACTERISATION D'ELECTROLYTES DE ZIRCONIA SUSCEPTIBLES D'ETRE EMPLOYES DANS LES SYSTEMES DE CONVERSION D'ENERGIE

par

T.A. Wheat*

RESUME

Le présent rapport fait partie intégrante d'un programme de perfectionnement des matériaux conducteurs ioniques susceptibles d'être employés pour l'emmagasinage de l'énergie et les systèmes de conversion d'énergie. Ces matériaux jouent un rôle de plus en plus important dans les travaux de perfectionnement des dispositifs d'emmagasinage et de conversion ayant des applications dans les piles à haute densité, les générateurs magnéto-hydrodynamiques (GMH), les piles à combustibles et les détecteurs.

Le zirconia est probablement le plus utilisé des 30 matériaux conducteurs ioniques à l'état solide connus. A cause de ses propriétés souhaitables notamment la nature réfractaire, la haute résistance mécanique et la haute conductivité électrique, ce matériau est un parfait aspirant pour l'usage dans les piles à combustibles et les générateurs GMH. Comme les données sont très limitées, particulièrement en ce que concerne les propriétés microstructurales, électriques et thermiques de ce matériau en fonction de son histoire thermique, une étude a été entreprise dans le but de déterminer la stabilité des diverses compositions dans le système $CaO-ZrO_2$ qui pourraient être appliquées aux piles à combustibles et GMH.

A l'aide d'un procédé chimique humide, on a préparé une série de compositions entre zéro et 22.2 % mol CaO. Elles ont ensuite été façonnées en échantillons frittés ayant une densité relative variant de 95% à 98%. Les échantillons frittés ont été préparés pour chaque composition ayant une géométrie convenant à la determination des caractérisques thermiques, électriques ou microstructurales. Le présent rapport ne touche que les aspects microstructuraux de la synthèse de la poudre et du développement des matériaux de frittage.

On a démontré, à l'aide des poudres réactives, homogènes et préparées chimiquement, que le zirconia cubique et monoclinique peut coexister dans les compositions contenant jusqu'à 10% mol de CaO. Entre 10

---

*Chercheur scientifique, Section de la céramique, Laboratoire des minéraux industriels, Laboratoires des sciences minérales, Centre canadien de la technologie des minéraux et de l'énergie, Energie, Mines et Ressources Canada, Ottawa.

et 20% mol de CaO, la phase cubique seulement est formée tandis qu'aux concentrations plus élevées de CaO la phase cubique coexiste avec le $CaZrO_3$. Lorsque la concentration du CaO augmente à plus de 10% mol, le système se transforme de deux phases à une phase et la grosseur des grains augmenté presque d'un ordre de grandeur.

On a trouvé que les matériaux entre 5 et 7.6% mol CaO subissent une grande contrainte au cours du stade de refroidissement du cycle thermique. En conséquence, ils subissent une expension progressive et irréversible durant chacun des cycles thermiques. L'importance de l'expansion est proportionnelle à la sévérité du choc thermique. La texture microstructurale de ces matériaux partiellement stabilisés est aussi fonction de l'histoire thermique. On peut donc prévoir une forte dépendance sur les propriétés électriques et thermiques.

CONTENTS

FIGURES

FIGURES (cont'd.)

FIGURES (cont'd.)

TABLES

INTRODUCTION

Although zirconia does occur in nature as the mineral baddeleyite, it is more commonly recovered from the mineral zircon ($ZrSiO_4$) which is available in large quantities principally in Brazil, U.S.A. (Florida), Australia (N.S.W.) and India (Travanacore). The production of the oxide itself exploits the reaction that occurs between zircon and alkali or alkaline earth hydroxides or carbonates at elevated temperatures, following which alkaline earth silicate is removed from the crushed fused product by washing. Other recovery processes depend on the formation of the volatile tetrachloride in a carbon-arc furnace or, alternatively, in an acid-leaching stage to produce the oxysulphate: calcination of either salt readily forms the oxide.

Unlike most materials, pure zirconia undergoes a disruptive volume change on heating, which formerly restricted its use in cycling temperature applications. This is due to the low-temperature monoclinic form transforming to the high-temperature tetragonal form between 900°C and 1100°C giving rise to a 3 vol % shrinkage on heating. By adding stabilizers such as calcia, magnesia or yttria, this anomalous effect can be controlled or eliminated.

From an historical point of view, it is fortuitous that much of the early recovery of zirconia involved calcium reactants. They tend to form a solid solution with the zirconia which may be stabilized in a cubic form, at >10 mol % CaO and hence are free of the disruptive monoclinic-tetragonal inversion. Also, during subsequent processing in which the material is formed and eventually fired to high strength bodies, the calcia in solution reacts with the residual silica, which is typically present at a concentration of 0.1 to 0.3 wt %, to form a calcium silicate grain-boundary phase. Although the exact composition of this material is unknown, it is important to realize in exploiting such a zirconia that eutectic compositions in the $CaO-SiO_2$ system have a melting point (mp) of 1436°C (34 wt % CaO) and 1460°C (56 wt % CaO) and that the compound $CaSiO_3$ has a mp of 1544°C. A typical example of such a grain-boundary phase formed in a commercial zirconia is shown in Fig. 1.

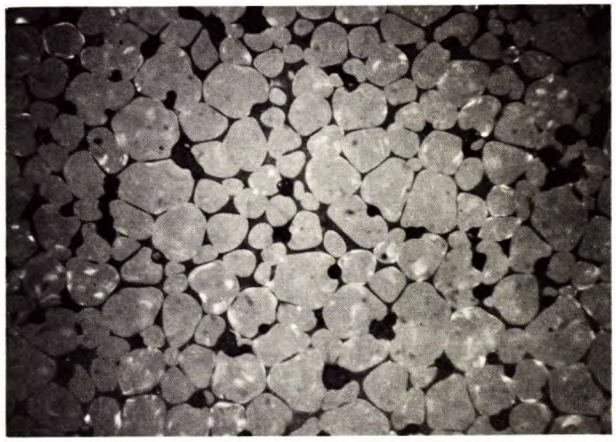

Fig. 1 - Typical microstructure developed by a commercially available zirconia. Light grey - zirconia; dark grey - silicate; black - pores.

The presence of calcium silicates in the zirconia microstructure has advantages and disadvantages. It allows this extremely refractory material, which may require up to 2000°C to develop a body having 95% theoretical density, to be sintered via a liquid-phase mechanism at relatively low temperatures, i.e., 1550°C, thereby producing a high-strength, glass-bonded product. In addition, the loss of some calcia from solution with the zirconia will also produce a two-phase system (monoclinic + cubic) that has markedly superior mechanical and thermal shock properties to either of the single-phase materials (1). However, the presence of a relatively low melting point silicate in the grain boundaries imparts poor under-load hot strength to the material and may also seriously interfere with the electrical properties of the bulk material. The potential for this to occur can be realized from

the reaction of 0.5 wt % silica in zirconia to produce ∿ 1 wt % calcium silicate if all the silica reacts and this will completely coat each grain in a body consisting of 20-μm spherical grains with a layer ∿ 34 nm thick. Consequently, there is a distinct possibility of having either the ionically conducting zirconia or the non-conducting silicate as the continuous phase in this two-phase system. Hence, it can be appreciated that a minor change in the silicate concentration or in its distribution could have a very marked effect on the electrical properties of the product.

In the past, the very refractory nature of the material and its very high thermal shock resistance led to its extensive use in the metallurgical processing industries. However, in the last 20 years it has been increasingly recognized that zirconia possesses useful electrical properties. Depending on composition and operating conditions, mainly temperature and oxygen partial pressure PO_2, zirconia can act as either an ionic or an electronic conductor, or both. In part both these conduction modes arise due to the development of a defective anion lattice in the calcia-zirconia solid solution (Fig. 2). Introducing a divalent stabilizing ion into the tetravalent cation lattice requires the development of vacancies in the anionic lattice to maintain electrical neutrality: in the fully stabilized material having between 10 and 20 mol % CaO, for every 2 mol % stabilizer added, 1 mol % oxygen vacancies are created.

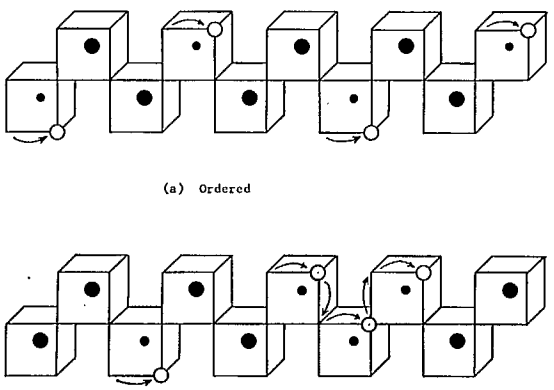

(a) Ordered

(b) Disordered

Fig. 2 - Schematic of the vacancy transport in ordered and disordered calcia-stabilized zirconia. Oxygen atoms are situated at the corners of all cubes. • Ca; ● Zr; O oxygen vacancy. After Carter and Roth (2).

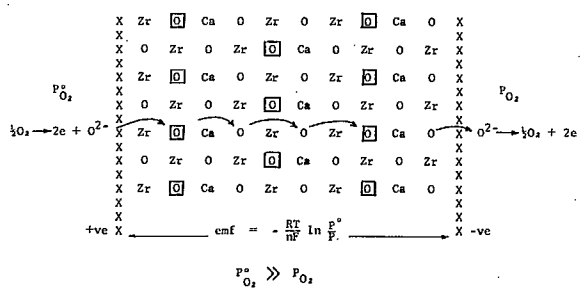

Fig. 3 - Schematic showing the development of an emf across a calcia-stabilized zirconia electrolyte in an oxygen concentration cell (fuel cell)

Ionic Conductivity

Due to the development of a defective oxygen lattice, the fully stabilized (cubic) materials exhibit high ionic conductivities as the oxygen ions become mobile and move by a hopping mechanism. The driving force for moving the ions through the electrolyte is the concentration gradient that is established across the zirconia (Fig. 3). In essence, this is the basis for a fuel cell - in practice, the gradient across the electrolyte is increased by the use of high and low PO_2 sources such as oxygen and hydrogen. In this manner gradients of 10^{10} to 10^{20} Pa/mm can be developed with a consequent increase in the emf generated.

From the Nernst equation (given in Fig. 3), where R = 1.9865 cal/mol/°K is the gas constant, F = 23,066 cal/V/mol is the Faraday constant and n = 4 is the number of electrons transferred per molecule of oxygen at T°K, it may be shown that a gradient of 10^{10} Pa will give rise to an emf of 0.631 V; increasing the gradient to 10^{20} Pa results in an emf of 1.262 V.

Electronic Conductivity

In the undoped, calcia-free material, electrons e' may be liberated either during the formation and ionization of thermally created oxygen vacancies, $V_o^{\cdot\cdot}$:

$$O_o \rightleftharpoons \tfrac{1}{2}O_2(g) + V_o^{\cdot\cdot} + 2e'$$

or during the formation of zirconium interstitials, Zr_i^{4+}:

$$O_o + Zr_o \rightleftharpoons \tfrac{1}{2}O_2 + Zr_i^{4+} + 4e'$$

where O_o and Zr_o are the neutral lattice atoms. Alternatively, electron holes, h', may arise either from the formation and ionization of zirconium vacancies, $V_{Zr}^{''''}$:

$$\tfrac{1}{2}O_2\ (g) \rightleftharpoons O_o + V_{Zr}^{''''} + 4h^{\cdot}$$

or from the formation and ionization of oxygen interstitials, O_i^{2-}:

$$\tfrac{1}{2}O_2\ (g) \rightleftharpoons O_i^{2-} + 2h^{\cdot}$$

Both types of conductivity may be induced in the same material, i.e., either stabilized (cubic) or unstabilized (monoclinic) zirconia depending on the temperature and the PO_2. For example, it has been reported that monoclinic zirconia is primarily an ionic conductor below 700°C and an electronic conductor between 700 and 1000°C for 10^{-17} Pa < PO_2 < 10^5 Pa (10^{-22} to 1 atm) (3). Each conduction mode is important in the two high-efficiency energy conversion systems: the magneto-hydrodynamic (MHD) generator (electronic or mixed conductivity preferred as pure ionic conductors tend to suffer severe electrochemical degradation under a high dc field) and the oxygen-based fuel cells (high ionic conductivity and low electronic conductivity required).

MHD Generator

As with any system for converting mechanical to electrical energy, this generator produces electrical power by the Faraday Law of Induction, i.e., electrical current is induced to flow in a conductor when it passes through a magnetic field. The major difference between the conventional and MHD generator is that, in the latter, the moving conductor is an electrically conductive, high-velocity plasma that passes down a duct and through a magnetic field as shown in Fig. 4. As a result, current is induced to flow across the plasma, through the electrodes set in the top and bottom of the duct and into the external circuit. After passing through the duct, the cooled gases are used in a conventional manner to also drive turbo-generators: power is derived from both the MHD generator "front end" and the turbine units at the "back end".

The great advantage of this dual system is its increased efficiency - where a conventional coal-fired thermal generating station may operate at approximately 35% overall efficiency, an MHD plant would be 50-55% efficient using the same fuel (4). Essentially, this increased efficiency results from the much higher operating temperature of the MHD unit. However, this higher temperature also exacts a heavy toll on the life of the material used to line the duct and form the electrodes and insulators. To date, this has proved to be the major limitation to utilizing MHD power generating systems.

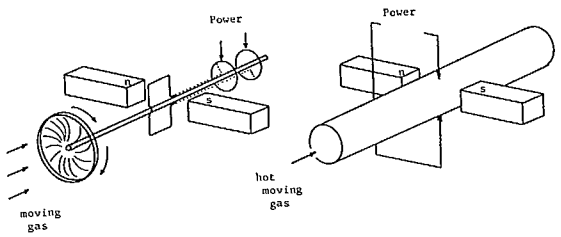

Fig. 4 - Schematic comparing the mode of operation of conventional and MHD generators

Conditions inside the duct during operation are severe: the flame temperature is well over 2000°C, i.e., nearly four times higher than in the conventional steam turbine. Assuming the generator is coal fired, the pulverized fuel is fed into the cone-shaped duct and expanded at high temperature to produce the plasma. The electrical conductivity is increased even further by adding seed material such as potassium, or preferably the more efficient cesium salt. Consequently, the duct lining has to be resistant to melting at the high operating temperature, to chemical attack by the very corrosive seed and coal ash present, and to general erosion by the coal particles which pass down the duct at velocities approximating mach 1.5.

Fortunately, the conditions are not as severe at the duct wall as it appears because an electrically conductive layer of coal slag builds up on the wall and this layer is exposed to the extreme conditions. By optimizing the fuel feed so that it contains additional slag, it is possible to balance the erosion of the slag from the walls with the rate of deposition from the flame.

Although the presence of a slag layer will afford some measure of protection under steady-state conditions, clearly the starting up or shutting down of a generator will impose severe conditions on the electrodes placed in the duct. These materials must be electrically conducting, extremely refractory, and stable to sudden temperature changes. A candidate material for electrode fabrication is zirconia.

Fuel Cells

In principle, all fuel cells operate by the reverse of electrolysis: fuel and an oxidizer are combined in the presence of a catalyst to generate direct current. This reaction may be exploited in a variety of cells which may use an acidic electrolyte (H_3PO_4), molten carbonate electrolytes, (Li_2CO_3-K_2CO_3-Na_2CO_3 eutectic mixture), a basic electrolyte (KOH), or a solid-state ceramic electrolyte such as those based on stabilized ZrO_2 or La_2O_3. Usually the fuel is either H_2 or a hydrocarbon obtained by conditioning either natural or process gas such as blast-furnace off-gas. Naphthas and other petroleum distillates can also be used. The oxidizer is either oxygen or air.

As an energy conversion system, the fuel cell has the advantage of high efficiency (~75%) at partial and full load. It is a silent and automatic device giving minimum pollution - the waste being either water or water + CO_2 depending on the fuel. In addition, considerable economic benefits can be realized in the use of modular units which allow distributed siting.

Recently, added interest has been given to further developing fuel-cell technology because of the possible future switch to a hydrogen-based economy. Using present technology, it has been estimated cheaper to transport energy in the form of CH_3OH (5) or H_2 (6) providing the distance is >500 km than to use the present high-voltage electrical transmission system. As a result, a second economic benefit would arise: with locally sited fuel cells, it would be possible to meet peak demand from the cells and augment the main base-load provided by the centrally located thermal generating stations. In turn, the present electrical transmission system would only have to meet the base-load demand - no additional capacity would be required to meet the peak loads. It has been estimated that a saving of approximately $220/kW of transmission system capacity would result (7).

The extensive exploitation of fuel cells has been limited by adverse economics which arise due to materials problems resulting in relatively short cell lifetimes. One problem concerns the gradual poisoning of the catalyst used at the electrodes. In practice, this poisoning effect can be reduced considerably by switching from low-temperature cells (acidic or basic electrolyte cells that operate between ambient and 200°C) to high-temperature cells based on the molten carbonate electrolyte operating at 600°C or the solid-state electrolytes that can operate up to 1000°C.

Such a high-temperature cell based on a

zirconia electrolyte is shown in Fig. 5. In typical hydrogen-oxygen fuel cells, the anodes are fabricated from porous platinum or nickel whereas porous platinum or silver is used at the cathodes.

An additional restriction is imposed on the design of a fuel cell. Because the zirconia has a conductivity of $\sim 2.10^{-2}$ $(ohm.cm)^{-1}$ at 1000°C, very thin plates or tubes must be used to reduce the total internal resistance of the cell. Consequently, this limitation places a severe demand on the electrolyte - it must withstand the thermal shock imposed on starting a cell from cold without developing any microcracks. Such cracks would allow the passage of molecular oxygen from one side of the cell to the other and thereby partially short circuit the cell.

From a safety viewpoint, the serious consequences of suddenly mixing large quantities of fuel and oxidizer at high temperature are minimized by cell design. A minor leakage is not important - molybdenum-wound furnaces have been successfully operated for years up to 1750°C using a protective H_2 atmosphere around the elements, which are contained within high-alumina tubes. In time, with the loss of a minor amount of volatile glassy phase (typically Na_2SiO_3 and K_2SiO_3) from the grain boundaries, the tubes become porous and allow the passage of oxygen into the hydrogen atmosphere. The presence of water in the outlet from these tubes is a reliable indicator that the furnace will probably fail within 24 h at 1700°C. Total failure is not catastrophic - the rapid ingress of oxygen to the elements is only indicated by the sudden emission of MoO_3 smoke from one or more of the elements.

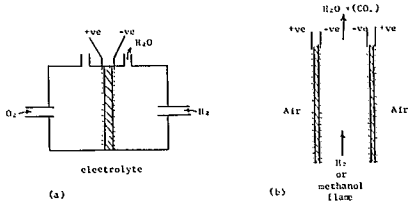

Fig. 5 - Schematic of fuel cells that exploit the reaction: $H_2 + \frac{1}{2}O_2 = H_2O$. Current density curve after the data of Binder et al. (8).

From the foregoing, it will be appreciated that the general use of an impure zirconia in either an MHD electrode or fuel cell electrolyte application will not be successful because both the electronic and ionic properties will be critically dependent on the concentration, composition and distribution of the minor amount of grain-boundary phase. Consequently, a program was initiated in CANMET to produce homogeneous zirconia having a low impurity content which could be fabricated into high-strength material suitable for use in fuel cells and MHD applications.

This report describes the wet-chemical method employed to produce the high-quality raw materials in the $CaO-ZrO_2$ system, their subsequent processing into a state suitable for dry-pressing, and the sintering and subsequent characterization of the microstructures obtained. The thermal and electrical properties of these materials and their relationship to microstructure will be reported later.

EXPERIMENTAL PROCEDURE

In developing high-quality ceramic materials, it is necessary to control both the concentration and distribution of the impurities. Where the ceramic is to be used in an electrical application such control is crucial to the successful development of the product. This is particularly true in the semiconductor industry where concentrations of dopant added to the silicon wafers are a few parts per million. In that field, the control of such low concentrations and the assurance of a uniform distribution is vital to the electrical performance of the device.

It is doubtful that such close control is required in the present work. However, it is

clear that the more traditional methods for preparing ceramic powders, e.g., by ball-milling oxides or oxide precursors together, are unsuitable as they tend to contaminate the powders with debris from the milling media and are unable to produce truly homogeneous materials. Consequently, a wet-chemical process was used.

In general, available wet-processing techniques for preparing reactive and homogeneous raw materials depend on either co-precipitation from organic or inorganic precursors or, alternatively, spray-freezing and freeze-drying an aqueous mixture of inorganic salts using the method of Schnettler et al. (9).

The so-called co-precipitation technique, using inorganic (10) or organic (11) precursors, has been employed for some time on an industrial scale to produce homogeneous, finely-divided ceramic raw materials for piezoelectric applications. However, it is misleading to claim that these methods involve a genuine co-precipitation procedure - the process inevitably involves a sequential precipitation as no two materials react at the same rate. This effect is particulary acute if organic precursors are used where steric hindrance may be significant. For example, the precipitation of silica by the hydrolysis of silicon tetra-ethoxide takes several hours at 100°C with a catalyst, whereas the formation of an alumina gel from the iso-propoxide is extremely rapid at room temperature without any catalyst (12). This problem of segregation due to widely differing precipitation rates does not arise in the spray-freeze/freeze-dry method. Consequently, the cryogenic technique was adopted for the present work.

Previous work has shown that it is impossible to form pure or doped zirconia directly using the cryogenic process because a frozen zirconyl salt gradually melts at -40°C (the lower limit of a commercial freeze drier) (13). As a result, the basic method given by Schnettler et al. (9) was modified to that shown in Fig. 6. In essence, the zirconyl ion was effectively removed from solution by precipitating a finely-divided zirconium hydroxide. The precipitate was washed to remove soluble salts and subsequently doped with a known amount of calcium formate solution. The resulting slurry was rapidly frozen and successfully freeze dried at -5°C without any of the previous difficulties. Details for producing these homogeneous and highly reactive zirconia raw materials has been reported elsewhere (14, 15).

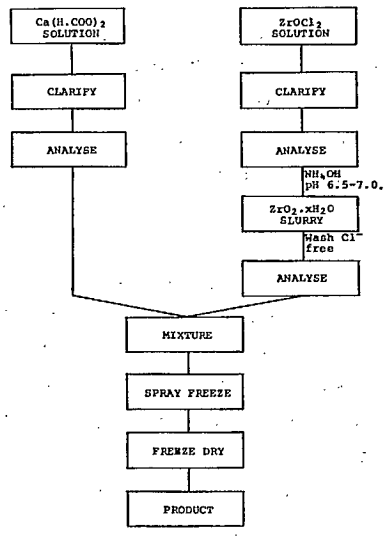

Fig. 6 - General flow sheet for the preparation of lime-stabilized zirconia powders

It appears at first sight that this method should result in a heterogeneous mixture because the zirconia component is first precipitated and the CaO precursor is later added as a soluble salt. However, it has been shown that by using dilute solutions of the reagents $ZrOCl_2$ and NH_4OH, the $ZrO(OH)_2.nH_2O$ precipitate is formed with a high surface area and as a result it adsorbs ~60% of the Ca^{2+} ions from the initial calcium formate solution within the first ten minutes. After spray freezing and freeze drying, the surface conditions of the precipitate have changed so that only ~20% of the Ca^{2+} ions may be recovered into solution on reslurrying the dried powder, i.e., after drying, 80% of the Ca^{2+} ions remain adsorbed on the precip-

itate surface (15). As a result of this extensive adsorption, the reaction path of the doped powders does not follow that of the separate components. Instead of having a sequence in which the ZrO_2 powder crystallizes at 450 to 550°C, depending on the CaO content, and the formate decomposes at ~500°C to first form the carbonate which further decomposes to the oxide between 800 and 900°C and finally reacts with the ZrO_2 to form a solid solution above 900°C, most of the reactions to form the solid solution are composed by ~550°C.

In essence, the reaction path follows two routes depending on the CaO concentration. Where the CaO content is less than 11.5 mol %, all the formate decomposes directly to the oxide between 300 and 400°C. As the temperature increases further, the amorphous ZrO_2 crystallizes rapidly and simultaneously reacts with the CaO present to form the solid solution betwwen 450 and 550°C - the higher temperature being with the higher CaO concentration. Where the CaO content is >11.5 mol %, 93 to 95% of the formate present decomposes directly to the oxide between 450 and 550°C, while the remaining ~6% formate forms the carbonate. Consequently, between ~500 and ~700°C the solid solution co-exists with a low concentration of $CaCO_3$. As the temperature is increased, the carbonate finally decomposes to the oxide which then enters into complete solid solution with the ZrO_2 at ~700°C. The reaction sequence for materials so prepared is given in Fig. 7 (14, 15).

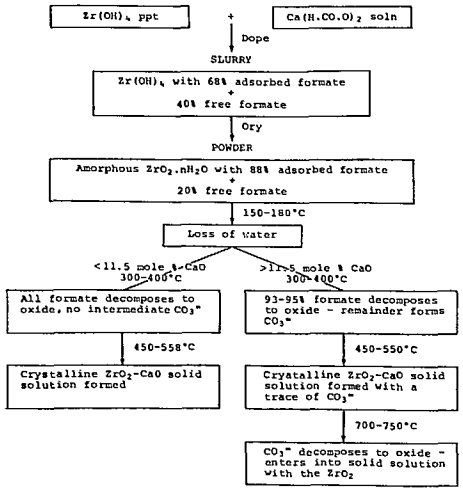

Fig. 7 - Summary of reactions occurring during the preparation and calcination of zirconia powders

RESULTS AND DISCUSSION

Characterization of Raw Materials

The as-prepared materials were all bulky, free-flowing, amorphous, white powders having a tap density of ~150 kg/m^3. Due to the presence of both calcium formate and adsorbed and absorbed water, the powders required a calcination stage to remove the volatiles H_2O, CO_2 and CO prior to forming and firing. If this calcination is done using simple fixed-set-point furnace facilities, it is possible that the powders will be heated at a rate of 25°C/min between 400 and 600°C, i.e., through the temperature of crystallization. Under these conditions it is likely that the newly formed crystallites will grow very rapidly and this, in turn, will lead to a defective structure probably containing many vacancies. With further heating, the vacancies would be expected to coalesce and form a micropore within each crystallite. During subsequent sintering, it will be impossible to eliminate all the porosity arising from this source because, in some cases, the original crystallite will be the nucleus of the final crystal in the sintered body and hence the grain boundary would be moving away from the original micropore and thus unable to act as a vacancy sink. As a result, it is impossible to form a theoretically dense product.

Differential Thermal Analyses (DTA) and Powder Calcination

To minimize the formation of microporous crystallites, the powders were calcined in air using a heating rate of 200°C/h to 10°C below the crystallization temperature of 450 to 550°C, given by the differential thermal analyses (DTA) shown in Fig. 8, 9, and 10. There-

after, the temperature increased at 3°C/h to 15°C above the crystallization temperature. The additional ∿400°C up to the final calcination temperature was gained at a heating rate of 20°C/h.

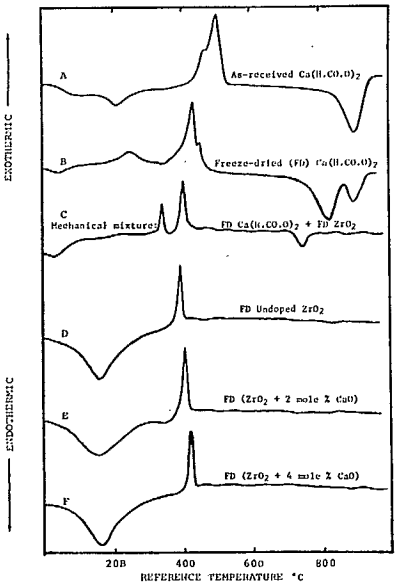

Fig. 8 - DTA curves of calcium formate and as-prepared zirconia samples heated at 12°C/min

It has been shown previously that the surface area of these powders is dependent on both the calcination temperature and the concentration of CaO - the greater the CaO content, the higher is the surface area at any given temperature between 600 and 1200°C (14, 15). To preserve the intrinsic reactivity of these materials, it is desirable to calcine to a temperature that will develop a surface area of ∿20 m^2/g. However, because of the combined effects of CaO content and temperature on surface area, it is impossible to predict the temperature at which each composition should be calcined to produce a 20 m^2/g surface area. Consequently, trial calcinations were conducted at selected temperatures between 850°C and 1000°C; the samples being heated in air at the given temperature for 1 h. The results are given at Table 1.

From the preliminary data in Table 1, it was decided to calcine the powders at either 910, 950 or 960°C for 1 h in air. Consequently, a number of different compositions could be calcined simultaneously. After calcining at the selected temperatures and slow heating rate dis-

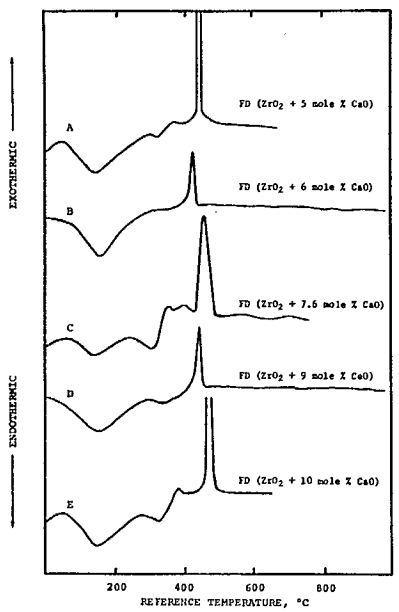

Fig. 9 - DTA curves of as-prepared zirconia powders containing between 5 and 10 mol % CaO heated at 12°C/min

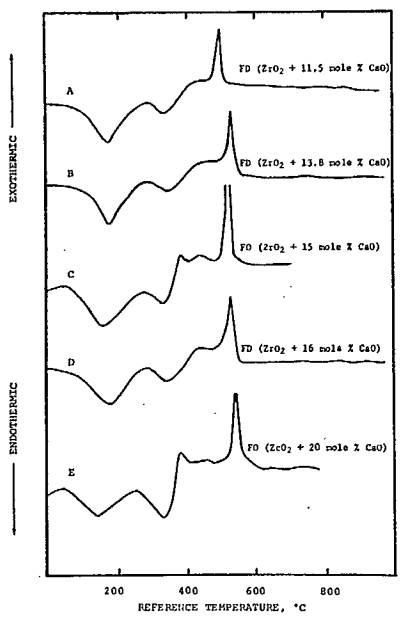

Fig.10 - DTA curves of as-prepared zirconia powders containing between 11.5 and 20 mol % CaO heated at 12°C/min

Table 1 - Variation of surface area with calcination temperature for undoped and doped zirconia

Composition mol % CaO	Surface Area m^2/g	Temperature °C
Undoped	36.20	850
	31.75	900
	19.80*	925
	11.93	950
	10.49	975
5	25.97	900
	27.31	950
	24.30	950
	22.50*	975
	22.00	1000
7.6	28.80	950
	26.35	975
	23.66*	1000
10	27.26	950
	21.05*	975
	19.96	1000
15	26.15	975
	19.23*	1000
20	20.03*	975
	18.04	1000
22.2	17.90	950
	16.57	975

*Calcination conditions producing material having a surface area close to the target value of 20 m^2/g. However, it must be noted that the small samples used for the data above (~1 g) were heated at ~25°C/min, i.e., a total heating time of 45 min was used to raise the temperature from ambient to 1000°C. Because of the much slower heating rate required for the calcination of the main batch of ~300 g of material and the resulting longer time the material was exposed to elevated temperatures that promote crystallite growth, calcination temperatures slightly lower (~10°C) than those indicated above by * were used.

cussed above, the surface area was again determined. The results in Table 2 show that, in general, a value close to 20 m^2/g was obtained.

It can be shown that the relationship between surface area and particle size is given by:

$$\text{Surface area } (m^2/g) = 6p^2/d \times p^3$$

when the material is assumed to be composed of cubic-shaped particles that are theoretically dense and have an edge length of p cm (15). Assuming the density, d, of zirconia is 6000 kg/m^3 then a surface area of 20 m^2/g suggests a particle size of ~50 nm (500 Å). However, the development of material having such an extremely small crystal size does not guarantee that it can be formed and subsequently fired into high-density bodies. In practice, the opposite tends to be true as such materials are frequently very difficult to form by conventional pressing techniques without modifications being made to the powder - they readily crack and "cap" or laminate adjacent to punch face. Even if formable, they are usually badly agglomerated powders. Consequently, the "memory" of the agglomerate size and shape in the loose powder, retained from the original spherical morphology developed in the spray-freezing stage, is retained in both the green-pressed and fired body. This effect is clearly shown in Fig. 11; the dense, circular areas shown in the fired material are

Table 2 - Surface area of zirconia after very slow calcination

Composition mol % CaO	Surface Area m^2/g	Temperature °C
Undoped	13.36	910
5	22.75	960
7.6	24.94	960
10	20.01	950
15	19.31	950
20	19.06	950
22.2	19.68	910

(a) 400 μm

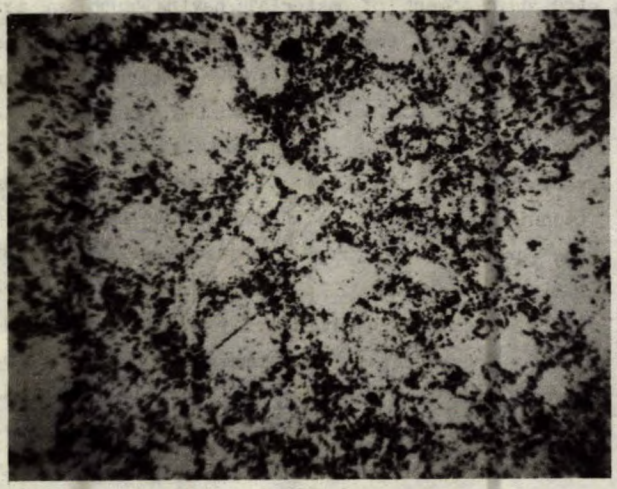

(b) 400 μm

Fig. 11 - Microstructure of 16 mol % material (a) Powder viewed in transmitted light (b) Sintered body formed from (a) pressed at 70 MPa and fired to 1485°C viewed in reflected light

essentially the same size and shape as the agglomerates in the calcined powder. Removal of the larger spheres from the powder by screening through a 325-mesh sieve results in the microstructure shown in Fig. 12; the pore distribution is more uniform and no dense circular areas are formed.

Materials having a high surface area also tend to adsorb H_2O and CO_2 from the atmosphere, forming surface complexes that may be stable to 600°C or more. In preparing Y_2O_3-stabilized ZrO_2 by the so-called co-precipitation of the hydroxides, it has been reported that carbonate complexes are formed which decompose on "... calcination, liberating CO_2 some of which is trapped in voids formed by microsintering" (16). Because of this effect, the authors found that their material would sinter to a density of only ~90% theoretical at 1800°C for 12 h.

While the adsorption of CO_2 undoubtedly occurs in the present materials (15) it would not be expected to produce 10% porosity in a compact. The effect of CO_2 adsorption would only be expected to control the final stages of sintering between 98 and 100% density. It is probable that the authors overlooked the far more significant effect arising from badly agglomerated raw materials: their only attempt to disperse the powders was that they "... were ground to pass 200 mesh using plastic containers and spheres".

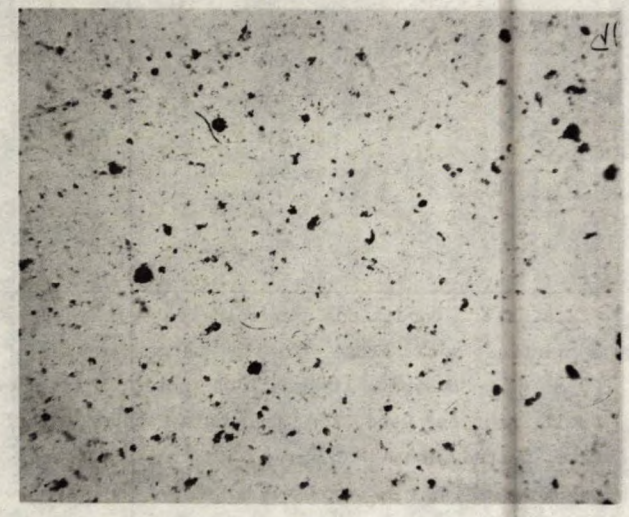

400 μm

Fig. 12 - Microstructure formed by minus 325-mesh fraction of 16 mol % material pressed under 70 MPa and fired to 1485°C with no soaking period

Powder Deagglomeration

The effect of severe agglomeration in any type of wet-chemically prepared raw material will prevent the formation of high-density bodies on sintering. For example, in the present work, material calcined at ∿1000°C for 1 h and uniaxially pressed at 70 MPa followed by firing at 200°C/h to 1500°C with no soaking period resulted in samples having a relative density of only 83%. Attempts were unsuccessful to increase the fired density by increasing the green density through the use of higher forming pressures, up to 350 MPa, which it was anticipated might collapse the spherical agglomerates. The spheres did not collapse, the fired density was raised only slightly to 87% at 350 MPa, and the samples developed either microcracks or complete laminations in the green state at >210 MPa. As shown in Fig. 12, some means of developing a more uniform microstructure is needed. It appears necessary to incorporate a powder lubricant into the powder to allow the particles to slide over each other during pressing. The large pore pockets shown in Fig. 12 are probably due to particle bridging occurring during forming. It would also be desirable to include a powder binder in the system so that relatively high forming pressures up to 350 MPa could be used without the risk of developing either microcracks or complete laminations in the pressed materials.

As shown earlier, a mixture of 5.5 wt % polyvinyl acetate* binder and 1.5 wt % polyethylene glycol** lubricant is effective in promoting a uniform green and fired microstructure in cryochemically prepared raw materials (15, 18). Consequently, the materials prepared in the present work were similarly treated. In essence, the calcined powders were ball milled in a plastic mill using high-alumina milling media and methanol containing dissolved Gelva V-7 and Carbowax 400. After milling for 1 h to break down most agglomerates and to disperse the additives, the slurry was spray dried in a Nerco-Niro drier using a spinning disc atomizer and operated at an inlet temperature of 150°C and an outlet temperature of 75°C. The product was composed of uniform ∿20-μm diam spheres which imparted nearly free-flowing characteristics to the powder.

The difficulty in breaking down agglomerates is shown indirectly by the particle-size distribution in the slurry obtained after 1-h milling in methanol. Fig. 13 shows the typical distribution developed in all the compositions prepared. Despite the apparently fragile nature of the spheres in the calcined material (note the debris from the broken agglomerates covering the surface of the material shown in Fig. 11a) it was not possible to lower the mean equivalent spherical diam below 4 μm. The distribution was the same with a standard deviation of 1.2 μm for all materials. After spray drying, the materials were composed of an essentially monosized distribution of ∿20-μm diam spheres as shown in Fig. 14.

Despite the retention of 4-μm agglomerates after milling and the subsequent formation of 20-μm agglomerates during spray drying, the combined effects of lubricant and binder and the small agglomerate size of <44-μm, were found to eliminate the "memory" effect (Fig. 12).

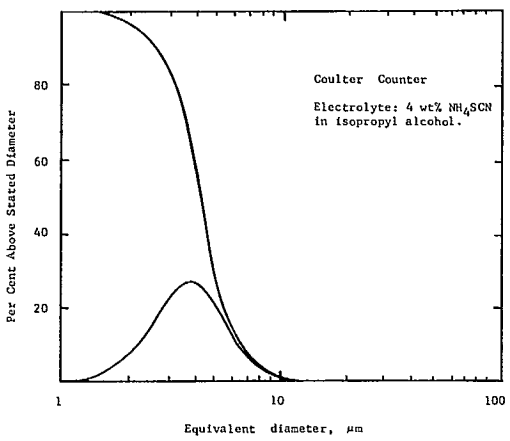

Fig. 13 - Typical particle size distribution of calcined material after ball milling in methanol for 1 h

* Gelva V-7, Monsanto Canada Ltd., Montreal, Que.

** Carbowax 400, Union Carbide Canada Ltd., Toronto, Ont.

Fig. 14 - Typical morphology of calcined materials after spray drying - viewed in oblique illumination

Dense spherical zones were no longer retained in the green or fired microstructures or samples fabricated using calcined material to which the binder and lubricant had been added.

Electron Microscopy

The general pore and crystallite size in the calcined materials was determined using either scanning or transmission electron microscopy (SEM or TEM). The fine porosity and general spherical form of the spray-dried agglomerates were confirmed by an SEM examination of each powder. Typical structures of various compositions are shown in Fig. 15 and 16. Although the 20-µm diam size of the spherical particles is confirmed, it can be seen that considerable variation exists in the amount of material that retains this spherical form. This is particularly noticeable between the mostly fragmented morphology of the 10- and 22.2-mol % materials and the more perfect form of the 15-mol % sample.

It has been shown by others that if a finely dispersed non-porous particulate powder having a surface area of 1 m^2/g is treated with 1 wt % of any binder, then the additive is readily observed in SEM micrographs (17). However, in the present work, despite the use of an unusually high concentration of organic additives of 7 wt % to impart desirable pressing characteristics, no evidence of these was observed in the SEM micrographs which confirms that the organic constituents were well dispersed throughout these porous, high surface-area powders. It is for this reason that the undesirable powder morphology could be eliminated in the green pressing stage of the fabrication process. Without the presence of the well-dispersed additives, the spherical morphology is retained throughout all subsequent processing leading to porous sintered material having a density of only ~84% of the theoretical value. Such material is valueless as an electrolyte in application due to the presence of an open pore system and is of little value in determining the intrinsic properties of the sample. There is still no universal agreement on the mathematical model that should be used to compensate for the presence of pores in determining the intrinsic electrical, mechanical or thermophysical properties from the data obtained for porous samples.

To examine the morphology of the crystals present in these spherical agglomerates, each composition was examined using a TEM. Specimens were prepared by first removing the organic additives from a small sample by heating the powder in air to 475°C for 1 h. (DTA established that the additives were lost at 260 and 340°C with no losses above 450°C). Each composition was then dispersed in HCl of pH 1 using an ultrasonic probe. To avoid the problem of particles charging-up in the electron beam of a TEM and moving around on the support grid, the HCl contained a small quantity of 2% formvar in chloroform. One drop of the dispersed suspension was placed on a carbon film held on a 150-mesh copper support grid and allowed to dry. The samples were examined in bright field using a Philip's EM300 microscope operated at 100 kV.

This examination was to determine whether the crystal morphology of the powders changed as a function of the increasing CaO content. Typical examples of the micrographs of

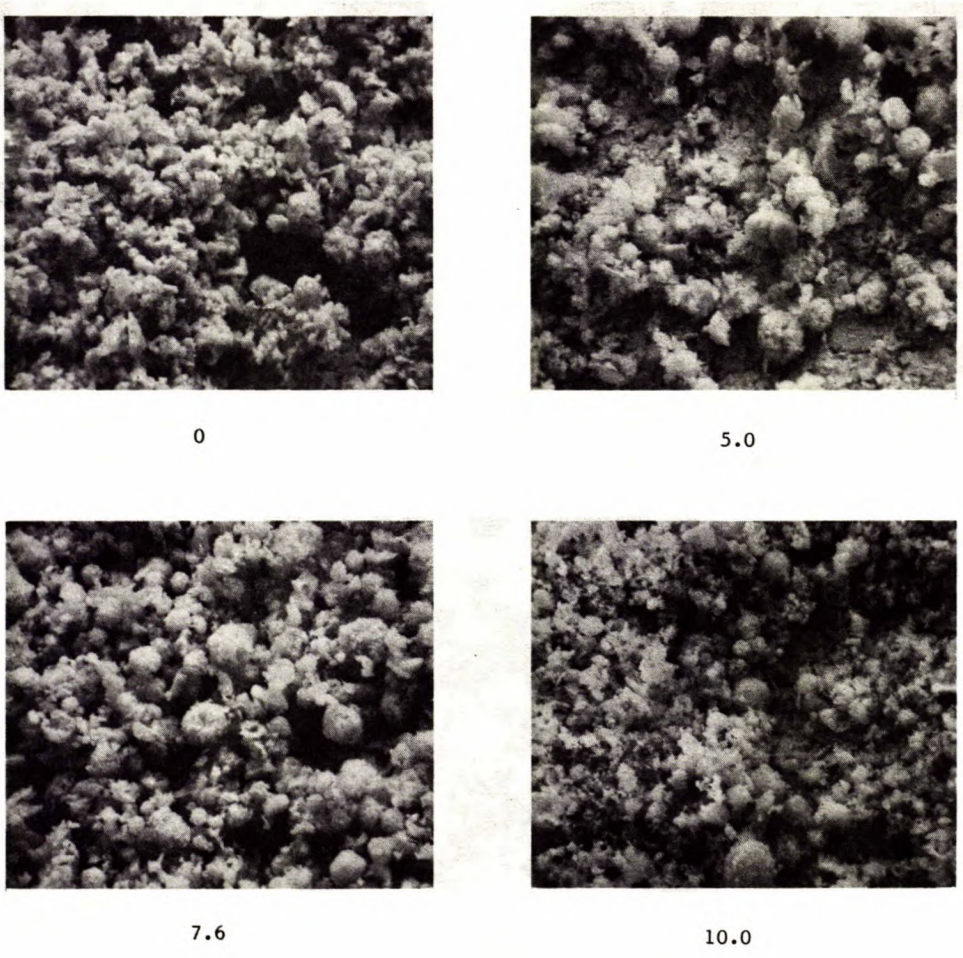

Fig. 15 - SEM micrographs of zirconia powders after spray drying with polyvinyl acetate binder and polyethylene glycol lubricant. The mol % concentration of CaO dopant in each sample is given.

each composition are shown in Fig. 17. It can be seen that the powders still retain a considerable degree of agglomeration despite the use of ultrasonic dispersion and a pH that effectively neutralizes the surface charge on the particles. The individual crystallites have the form of facetted spheres and a diameter of ~30 nm (300 Å) which agrees well with the value of 50 nm (500 Å) derived from the surface-area data of Table 2.

Closer examination of the powders reveals the reason for the apparently strong tendency to agglomerate. As shown in Fig. 18, the individual crystallites exhibit "neck growth" at the point of contact indicating that they are starting to sinter together, i.e., the powders really require milling to obtain fully dispersed material. This illustrates one of the difficulties in successfully fabricating bodies from such reactive raw materials. It is desirable to use material that will disperse readily when calcined at low temperature and it is also necessary that the crystallites be large enough when calcined at

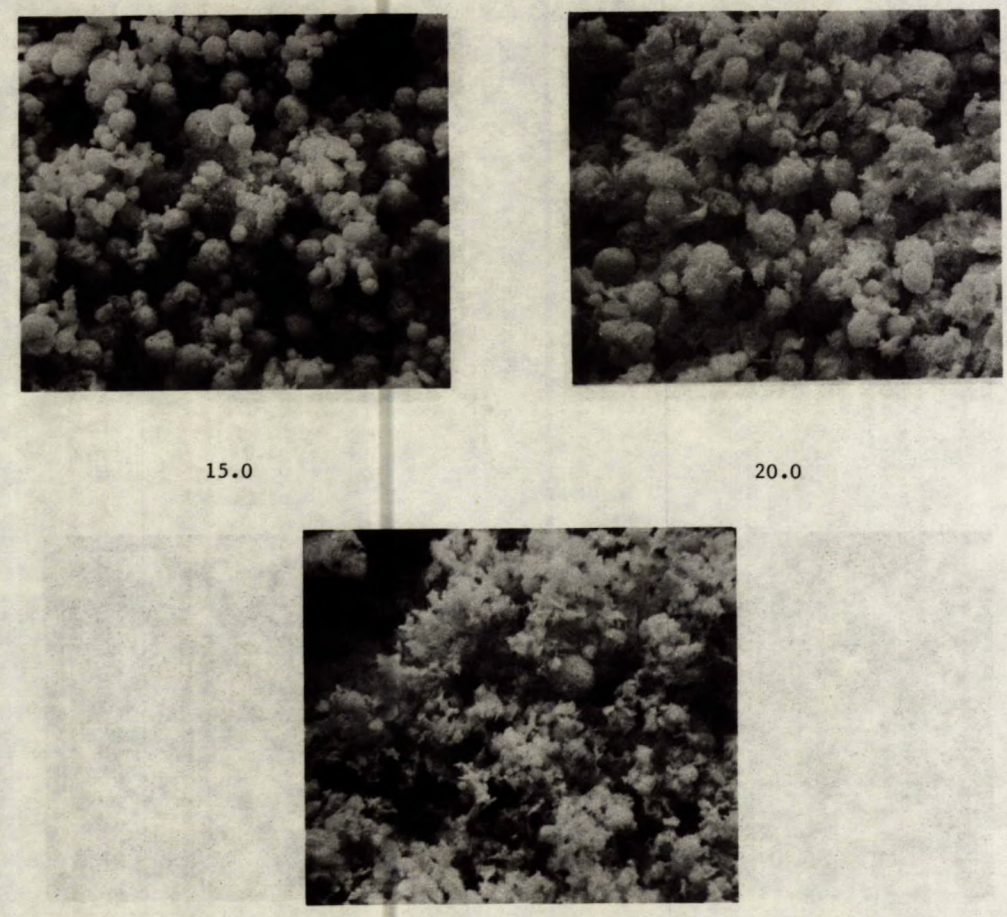

Fig. 16 - SEM micrographs of zirconia powders after spray drying with polyvinyl acetate binder and polyethylene glycol lubricant. The mol % concentration of CaO dopant in each sample is given.

high temperature to avoid a sudden grain growth during the sintering stage without sacrificing too much reactivity. In practice, the choice of calcination temperatures proved to be appropriate - high density material was successfully produced using a conventional dry-pressing and air-sintering process.

Fabrication of Green Materials

To meet the limitations imposed by the techniques used to determine the thermophysical and dielectric properties, a variety of sample sizes was required. For example, thermal conductivity studies require single right cylinders 25.4 mm in diam and 25.4 mm high, whereas thermal diffusivity data are obtained using seven discs 25.4 mm in diam and 6 to 9 mm high. To avoid too high an electrical capacitance, dielectric data are obtained on relatively thin discs 20 to 35 mm in diam and 2 to 3 mm thick.

From a fabrication point of view, the most difficult shape to produce using reactive

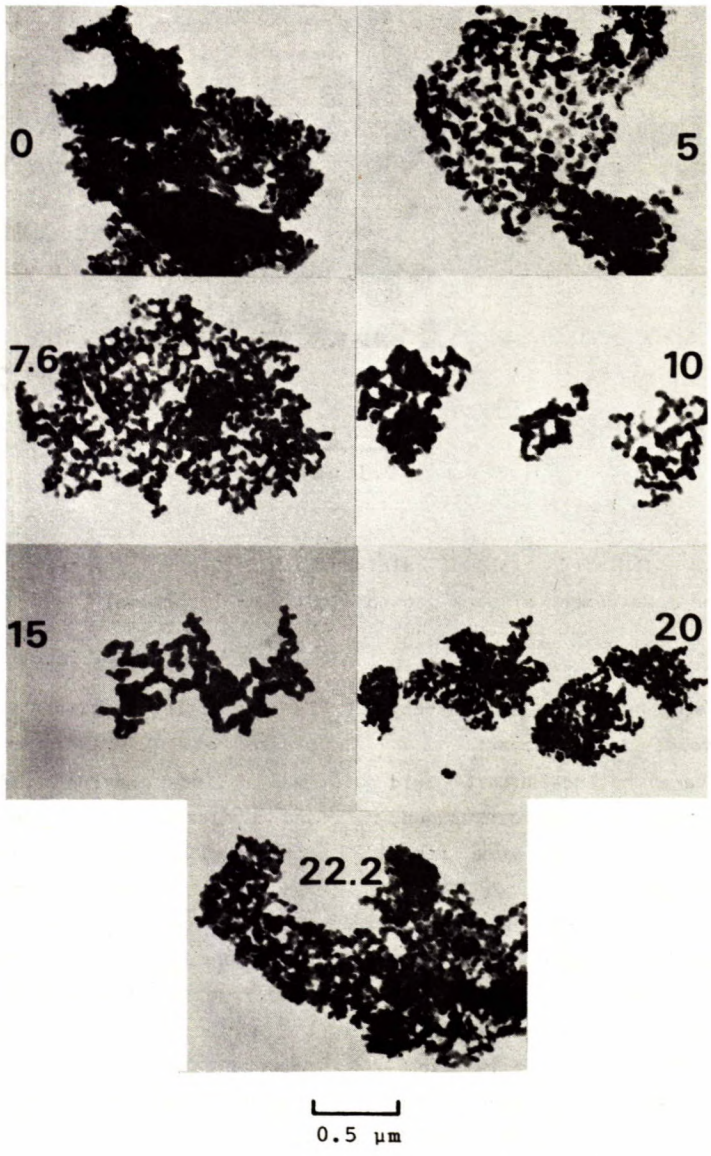

Fig. 17 - TEM micrographs of calcined powders viewed in bright field illumination. The mol % concentration of CaO dopant in each sample is given.

powders with a high firing shrinkage is that of the large equiaxed cylinder. In initial trials, in which the binder-containing powder was simply pressed and fired, radial cracks were common in the sintered body, as shown in Fig. 19. Consequently, for the large samples it was first necessary to form a green cylinder having as high a density as possible so that the firing shrinkage could be reduced and the potential to form firing stresses in the body would be reduced.

Powder Granulation

Immediately after the spray-drying stage, the powders were very well dispersed, with a tap density of $\sim$300 kg/m^3. To increase this value and thereby reduce the firing shrinkage, all the compositions were first pre-pressed and subsequently reduced to powder so that relatively high-density powder granules were formed. This would allow an increase in the pressed density of the final body yet would be weak enough

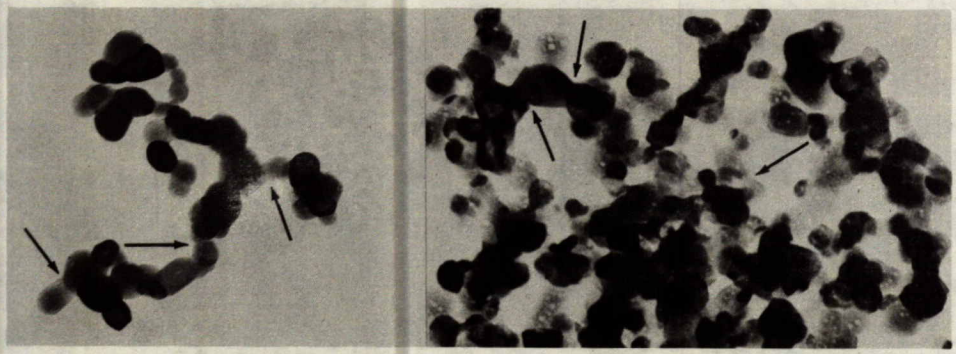

Fig. 18 - TEM micrographs of calcined 15 and 22.2 mol % material showing the development of neck growth (indicated by arrows)

to flow during the pressing operation and thereby avoid the formation of voids in the compact.

To produce sintered cylinders that could later be machined to the required dimensions, ∿135-g samples of each composition were first uniaxially pressed in a steel die at 28 MPa to produce a solid cylinder that could be handled. The sample was subsequently isostatically pressed at 210 MPa to produce a very hard body with a relative density of ∿48%. Each cylinder was then reduced to minus 200-mesh powder by machining in a lathe using tungsten carbide tipped cutting tools. Using two-way adhesive tape to support the material between live centres and an appropriate automatic cutting rate, it was found that more than 60% of the cuttings passed a 200-mesh screen. The remainder was hand-ground in an agate mortar until the entire batch of material was reduced to minus 200 mesh. The powder produced had a tap density between 1000 and 1400 kg/m^3 - there was no correlation between tap density and composition.

Powder Forming

Using the granulated powder, cylinders of each composition were first formed by pressing 130 g of material in a 44.45-mm diam steel die. The resulting cylinder was then isostatically pressed at 315 MPa to produce a nominally equiaxed cylinder having a relative density of ∿56% and a diameter of ∿38 mm. The minor amount of contamination that occurred on the surface from the steel die and from the rubber bag used in the isostatic pressing process was unimportant. Both the inorganic residue from the rubber and the iron from the die were subsequently removed from the surface by a diamond grinding stage that was necessary to produce the final geometry for determining the thermophysical properties.

Sintering Process

For the green pressed samples discussed above, two distinct parts of the sintering cycle were anticipated as potential sources of difficulty - the relatively low temperature binder-burnout stage between 150 and 600°C; and the region of rapid crystal growth occurring between 1000 and 1400°C. Difficulties could arise by using too high a heating rate in these two sensitive temperature ranges.

Binder Burnout Stage

To determine the temperature at which the organic additives present in the green com-

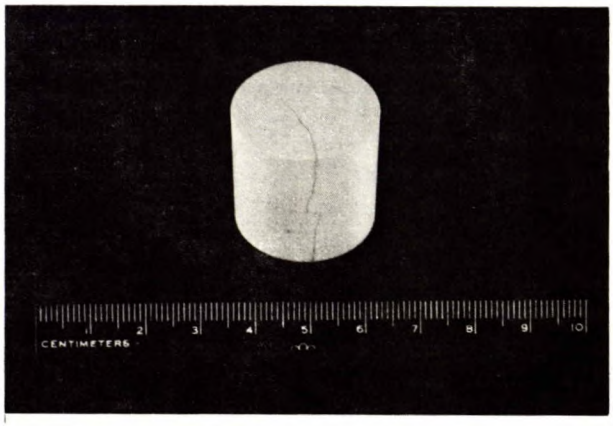

Fig. 19 - View of 10 mol % CaO material showing the presence of cracks in a sintered cylinder

pacts would begin to break down and eventually form CO_2 and H_2O, a DTA was conducted on a sample of the uncompacted powder using a heating rate of 12°C/min (Fig. 20).

It can be seen that there are three regions of activity - ~260, 340 and 370°C. As the reactions that occur during the pyrolysis of organic polymers are complex and can lead to the formation of various aliphatic aldehydes, ketones and acids as well as the lower members of the alkanes and alkenes, no attempt was made to identify the origin of the endothermic reactions detected by DTA. Because of the abnormally high concentration of organic additives used in the present materials and their use in forming samples having a relatively thick section, it was clear that a very slow heating rate would be required between 200 and 500°C of the sintering cycle. This would avoid cracking the samples due to the rapid internal formation of the final decomposition products, CO_2 and H_2O, at a time when the sample has its lowest strength.

An additional potential problem in removing binders from oxide ceramics during the early stages of sintering is the possibility of forming elemental carbon throughout the body that may be meta-stable up to temperatures >1000°C and eventually react with the host material to form CO_2 in the pores and produce a reduced matrix. The gas remains trapped, limiting the density that can be developed - the change in the valence state of the matrix can have a pronounced effect on the electrical properties of the product, e.g., the titanate-based capacitors. Although the formation of locally reduced material would not be significant in ZrO_2 as oxygen would readily migrate through the material and equilibrate the anion lattice, the presence of CO_2 at high temperature could dictate a lowered final density. Speculation elsewhere has indicated that the presence of CO_2 limited the development of high density in the sintering of Y_2O_3-stabilized ZrO_2 (16).

Sintering Stage

A further potential pitfall in the solid-state sintering of ceramic materials is to use too high a heating rate when the material is undergoing a rapid crystal growth. This is particularly true for very finely divided, high surface area material. In the present work, the green pressed compacts were fabricated from powder having a nominal surface area of 20 m^2/g and a particle size of 50 nm (500 Å) hence there is a considerable amount of free surface energy available to promote grain growth.

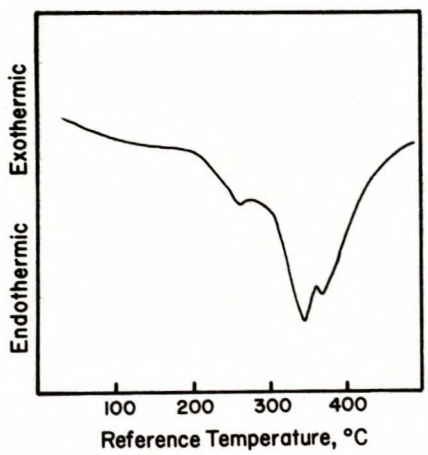

Fig. 20 - DTA curve of calcined powder containing 5 wt % polyvinyl acetate (Gelva V-7) and 2 wt % polyethylene glycol (Carbowax 400)

Ideally, the rate of grain growth and hence the rate of grain boundary migration should be slow enough to eliminate the residual closed pores as a grain boundary moves through the site of a pore. In practice, the situation is frequently different so that the boundaries move too rapidly to completely eliminate the pores in the initial sintering stages. With time, the grain size increases and the rate of boundary movement is reduced allowing the remaining pores to be intercepted by a grain boundary for sufficient time that the pore is removed. This mechanism leads to a microstructure in which pockets of closed pores remain at the centre of each grain whereas the grain edges are essentially pore free. An example of this type of microstructure is shown in Fig. 21.

In an attempt to determine the temperature at which sintering starts in the present materials, a series of samples of each composition was examined under a constant heating rate of 6°C/min using a Leitz Heating Microscope type IIA-P which is capable of operating in air up to 1750°C. The construction and operation of this equipment has been described in detail elsewhere (19). In essence, it allows the projected silhouette of a small sample to be recorded photographically with a progressively increasing temperature. Because the samples commonly have an irregular outline, it is necessary to use the square root of the projected area of the specimen as determined on a photographic enlargement to obtain the change and rate of change of length for each composition. Typical examples of the temperature-shrinkage characteristics of each are given in Fig. 22. Because of the similarity of the 5, 10 and 15 mol % materials, the data have been presented as one curve.

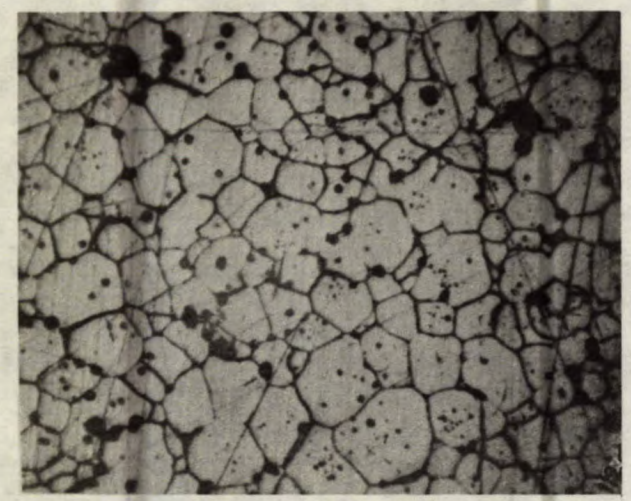

Fig. 21 - Typical microstructure developed in sintered 16 mol % material showing the tendency for the fine porosity to be located in the centre of each grain

It can be seen that up to 1000°C, all compositions behave similarly, exhibiting a nominally linear expansion from room temperature and having a mean expansion coefficient from 25 to 1000°C of 2.1×10^{-5}/°C. With the exception of the 20 mol % composition, the remaining materials start to densify between 1000 and 1050°C. The form of the densification curve between 1100 and 1600°C is the same for all the doped materials. There is no correlation between the total shrinkage observed and the composition because it is impossible to ensure that each sample has the same initial relative green density prior to heating - the samples being nominal 2-mm cubes. The inflection in the curve for the undoped material is due to the combination of shrinkage due to sintering and the additional shrinkage that accompanies the transformation of the low-temperature monoclinic phase to the high-temperature tetragonal form.

From the shrinkage data, it was clear that the maximum rate of shrinkage occurred between 1250 and 1300°C. Hence, it was necessary to use a very slow rate of heating through this temperature range during sintering. In practice, the need to meet the binder burnout requirements and the slow heating rate in the early stages of sintering was met by using a constant power input to the sintering furnace so that the initial heating rate of 10°C/min was gradually diminished as the equilibrium temperature of ~400°C was approached overnight.

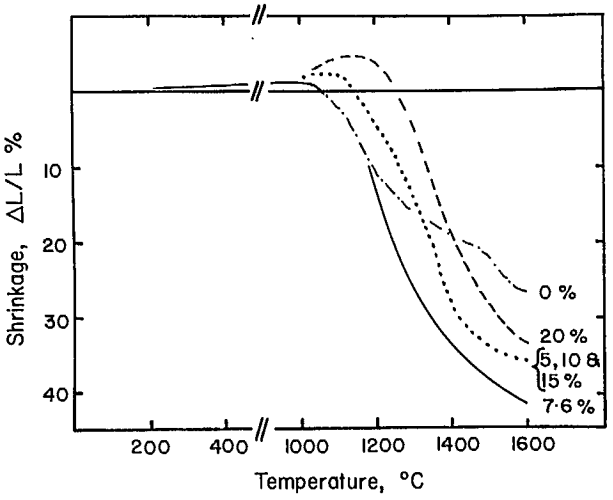

Fig. 22 - Shrinkage curves developed on sintering calcined material in air at 6°C/min

Although a temperature of 400°C in the DTA of Fig. 20 would suggest the presence of residual organic material, it should be noted that the DTA was obtained under dynamic conditions, 12°C/min, whereas during the sintering cycle the samples were maintained at 400°C for a minimum of 8 h. After this soak period, they were completely white and free from any organic residue.

From 400 to 1000°C, the temperature was increased at 25°C/h and maintained at 1000°C for 48 h. Thereafter, the temperature was increased at a variable rate decreasing from 3°C/min at 1000 to become 0.125°C/min at 1200°C. This very low heating rate was maintained up to 1550°C and the samples were held at this temperature for 6 h. Thereafter, they were cooled at 3°C/min down to 1100°C. At lower temperatures, the furnace followed its natural cooling rate that required an additional 16 h from 1100 to 150°C; the samples were removed at 150°C.

Characterization of Sintered Materials

The chief microstructural features of the sintered materials thought to be important in determining the intrinsic dielectric and thermophysical properties of these specimens were the phase composition, porosity and grain size. Consequently, only these characteristics were studied and, in each case, conventional techniques were found to be adequate.

X-ray Diffraction Analyses

The phase composition developed in the $CaO-ZrO_2$ samples prepared using the techniques described, has been given in detail elsewhere (15). Essentially, the monoclinic form that is stable at room temperature in the undoped material becomes progressively converted to the meta-stable cubic phase as the concentration of CaO is increased. At 10 mol % CaO, the samples become entirely cubic and this phase is maintained up to the limit of 20 mol % CaO. At higher concentrations, second phase $CaZrO_3$ is formed.

Above ~900°C, the monoclinic phase present in the partially stabilized samples having between 0 and 10 mol % CaO is transformed into the high-temperature tetragonal form. This particular phase change is unusual in that the monoclinic form experiences a shrinkage with increasing temperature as the tetragonal form develops. With a reduction in temperature, the reverse occurs - the tetragonal component expands in the gradually shrinking cubic matrix to produce domains of the monoclinic phase ~0.2 μm in diam. This behaviour gives rise to the phenomenon of "ratchetting" in which the material experiences an irreversible expansion with each cycle through the transformation temperature. For example, in material containing 7.6 mol % CaO, an expansion of 12% is developed during the first 15 cycles; thereafter, the material is stable to further thermal cycling.

The expansion of the CaO-free domains on cooling as the tetragonal phase is converted to the monoclinic form, leads to the development of a high density of microcracks throughout the bulk of the material which are thought to impart the exceedingly high thermal-shock resistance that is typical of the partially stabilized compositions. Previous work has shown that the 7.6 mol % ma-

terial can easily survive 35 cycles from room temperature to 1575°C and back to room temperature; it can also survive direct immersion in liquid steel at 1650°C when the heating rate is more than 400°C/s (18).

The presence of cracks in the partially stabilized samples could not be demonstrated by either optical or electron microscopy. However, their development can be inferred from the X-ray diffraction patterns of as-fired powder and as-fired compacts and the changes that accompany these samples with thermal cycling (Fig. 23).

It can be appreciated that compacts of the partially stabilized zirconia (PSZ) will be under considerable strain after firing, especially with the imposition of the 3 vol % expansion of the domains that occurs on cooling between 1100 and 900°C. The exposure of such a material to a sudden drastic thermal shock would not be expected to lead to an annealed structure, yet that is the interpretation of the data presented in Fig. 23. The alternative explanation that the cubic:monoclinic ratio changes with thermal history is difficult to accept in the present case. Figures 23A and 23B were obtained from material that received the same thermal treatment and would be expected to have the same phase ratio, yet the diffraction patterns are completely different.

It can be seen that as the compacted material suffers an increasing number of thermal shock cycles, the diffraction pattern changes and approaches that generated by the loose powder. This change is thought to be due to the release of strain in the microstructure following the development of a microcrack network and the irreversible expansion.

From these data it is clear that both the electrical and thermal properties of the PSZ materials containing 5 and 7.6 mol % CaO should be highly dependent on the thermal history of the samples used. It has been suggested elsewhere that the transition temperature for the monoclinic-to-tetragonal inversion can occur at abnormally low temperatures due to the presence of high stress in the microstructure: temperatures as low as 400°C have been found adequate for the transition and "ratchetting" to occur (19). Consequently, it is possible that irreproducible results could be obtained if the temperature were to exceed ~400°C, i.e., a hysteresis effect could occur in both the thermal and electrical properties of PSZ on raising the temperature from room temperature to 1000°C and back. Repeated cycling to high temperature would only make the situation worse. This possibility is of signi-

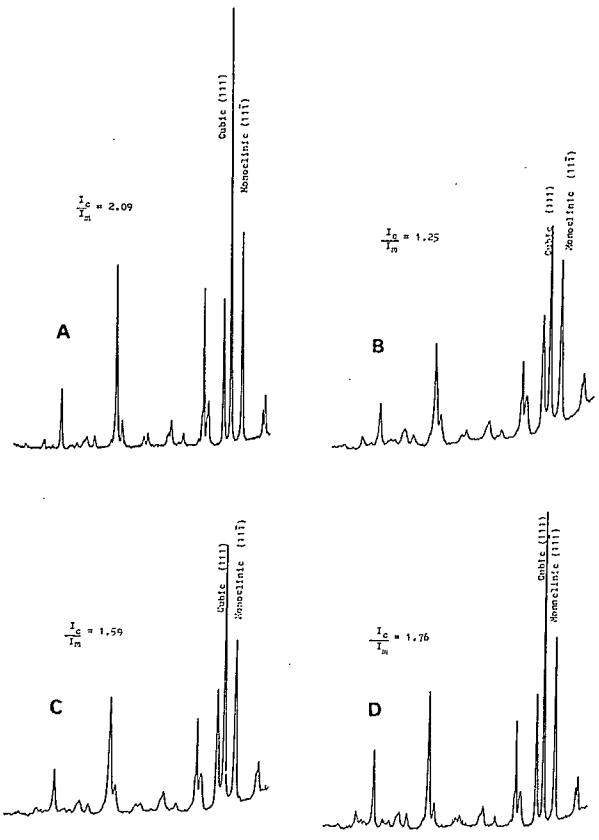

Fig. 23 - Comparison of microdensitometer traces of Guinier X-ray diffraction patterns obtained from partially stabilized 7.6 mol % material fired in air to 1500°C with no soak: A - As-fired powder B - As-fired compact C - Sample B thermally shocked once to 1575°C D - Sample B thermally shocked 35 times to 1575°C

ficance not only on a laboratory scale during the determination of properties but could also be of crucial importance in the commmercial application of zirconia in either fuel cells or an MHD duct. In both cases, a considerable thermal shock would be experienced by the material during service and this could lead to a much reduced upper limit of the current density capacity of the material.

Optical Microscopy

Because materials having between 10 and 20 mol % CaO stabilizer form a cubic phase on firing, examination of sintered samples in transmitted light would not yield much information on material that is generally very fine grained and isotropic. Consequently, samples were mounted and polished using a technique described elsewhere (20) and subsequently examined in reflected light using either partially crossed polars (0 to 10 mol % CaO) or a partially defocussed image of a relief-polished surface (10 to 20 mol % CaO) to reveal both the micro- and macro-porosity and the grain size. This method is quick and does not depend on the development of an etchant to show the grain structure; however, the image contrast is lower than that of an etched surface and hence it is sometimes difficult to obtain good photographs, particularly with fine-grained materials. Typical microstructures obtained in this manner are shown in Fig. 24 to 30.

In general, it can be seen that all the materials can be sintered to a high density. Comparison of the low magnification micrographs in Fig. 24(a) to 30(a) shows the presence of few pores (black features). The angular nature of those seen in the 5 and 10 mol % materials suggests that they are "pull-outs" (Fig. 25(a) and 27(a)). This possibility is also supported by the density data of the sintered compacts which showed that the total porosity of all the compacts was comparable and varied between 4 and 2%.

One of the unusual features of this series of compositions is the progressive increase in grain size as the CaO concentration increases to 20 mol % - at higher levels, a fine-grained size system is again formed. The undoped material has a grain size of ~4 μm, and this is only slightly increased with 5 mol % CaO. At 7.6 mol % CaO, a bimodal grain size distribution is developed in which the initial 4-μm grains are still present but accompanied by equiaxed grains of ~25 μm. At 10 mol % CaO, the structure is similar but the amount of fine-grained material is reduced. With the development of a single-phase material at 15 and

(a) 400 μm

(b) 100 μm

Fig. 24 - Microstructure developed in undoped zirconia after firing to 1550°C for 6 h

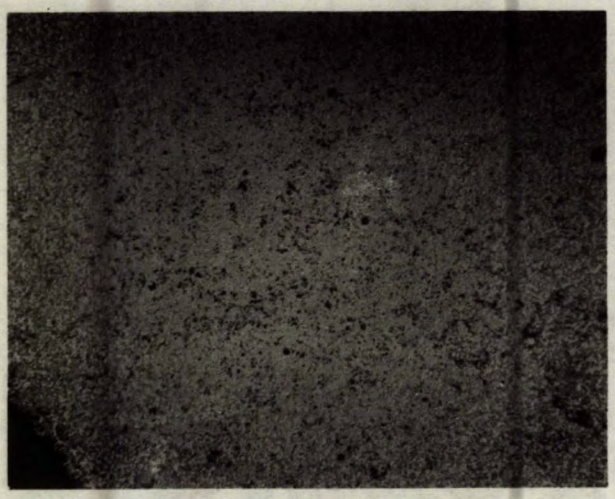

(a) 400 µm

(b) 100 µm

Fig. 25 - Microstructure developed in zirconia containing 5 mol % CaO after firing to 1550°C for 6 h

(a) 400 µm

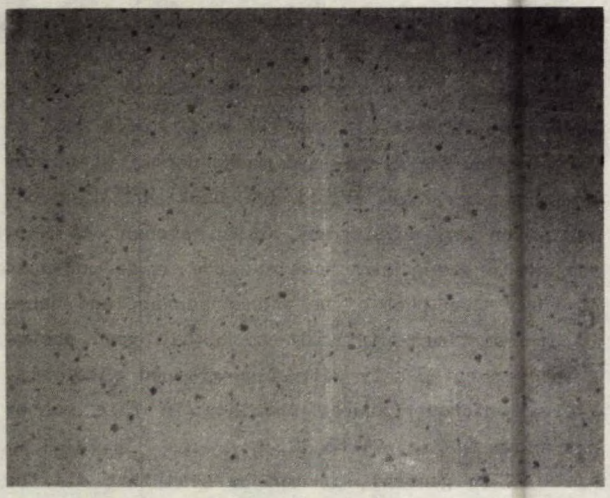

(b) 100 µm

Fig. 26 - Microstructure developed in zirconia containing 7.6 mol % CaO after firing to 1550°C for 6 h

20 mol % CaO, the microstructure is seen to consist of uniform, equiaxed grains of ~50 µm and ~40 µm respectively. At higher CaO levels, the system again becomes two phase as $CaZrO_3$ is formed in the presence of the cubic phase: coincident with this phase change, the grain size is also reduced.

Attempts made to fabricate samples of the undoped material to obtain electrical data on the monoclinic phase were unsuccessful. The discs broke into ~2-mm diam pieces and were badly fractured as shown in Fig. 24. Even a very slow cooling rate between 1100 and 900°C failed to prevent spontaneous fracturing as the high-

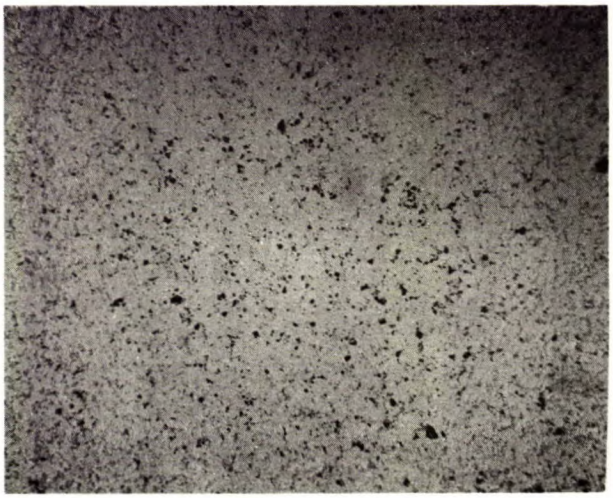

(a) 400 µm

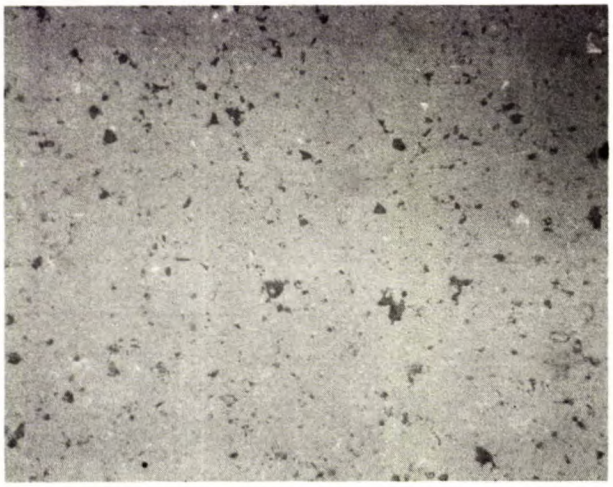

(b) 100 µm

Fig. 27 - Microstructure developed in zirconia containing 10 mol % CaO after firing to 1550°C for 6 h

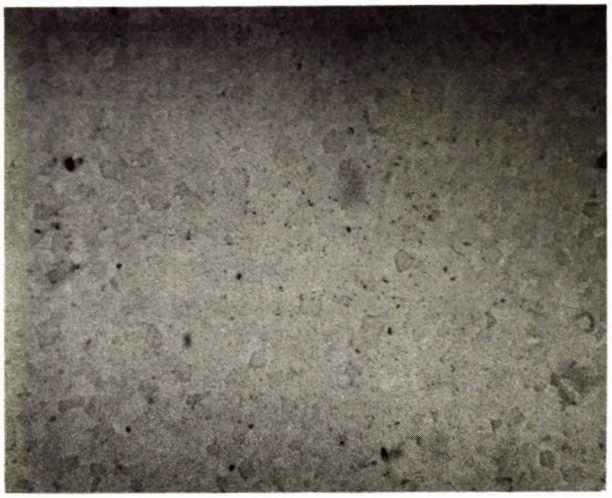

(a) 400 µm

(b) 100 µm

Fig. 28 - Microstructure developed in zirconia containing 15 mol % CaO after firing to 1550°C for 6 h

temperature tetragonal phase inverts and forms low-temperature stable monoclinic with a 3 vol % expansion.

Although the two-phase system (monoclinic + cubic) was shown by X-ray diffraction analysis to be developed in materials containing 5 and 7.6 mol % CaO, the polished sections failed to reveal the discrete phases. The apparent single-phase nature of the partially stabilized compositions has been observed previously and was attributed to the very finely divided nature of the monoclinic phase which is precipitated in the cubic matrix during cooling from the firing temperature (15). It has subsequently been shown by others that the precipitates are formed as thin rods having a length of ~0.1 µm (21), i.e.,

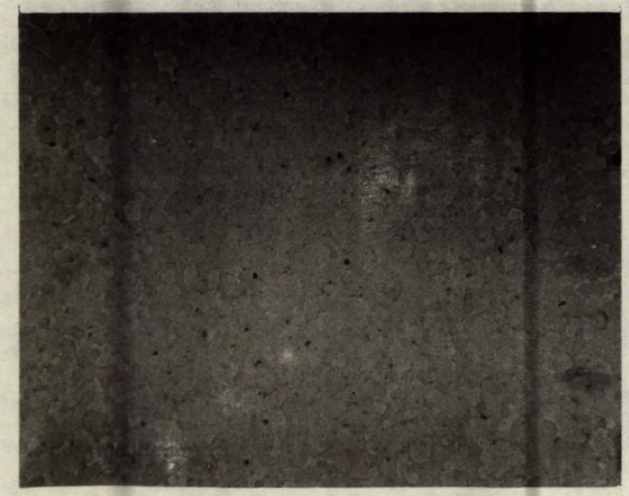

(a) 400 μm

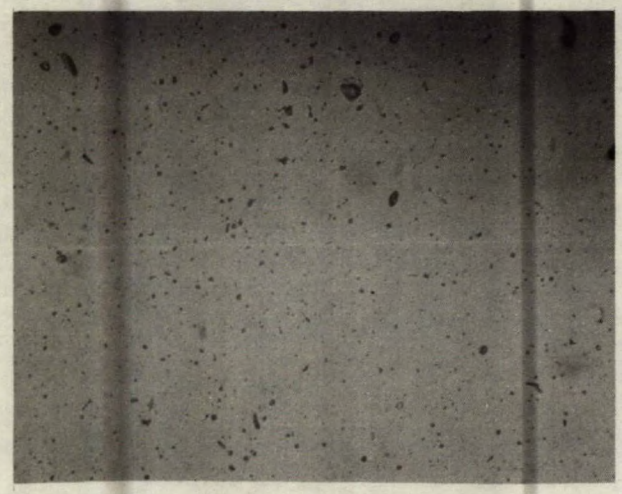

(b) 100 μm

Fig. 29 - Microstructure developed in zirconia containing 20 mol % CaO after firing to 1550°C for 6 h

(a) 400 μm

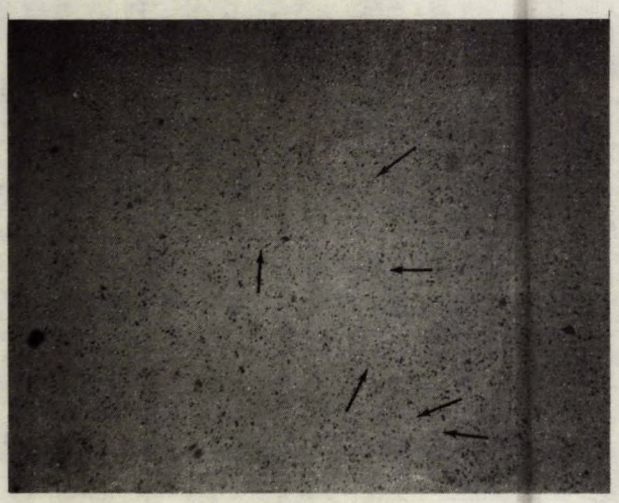

(b) 100 μm

Fig. 30 - Microstructure developed in zirconia containing 22.2 mol % CaO after firing to 1550°C for 6 h. Arrows indicate $CaZrO_3$ second phase

they are well below the resolution of the optical microscope.

It should be noted that the white features in the 10 mol % material, Figure 27(b), are subsurface reflections that probably arise from fractured grain boundaries. It may be significant that the materials that show these reflections are those that suffer the most "pullout" damage during polishing, i.e., they probably incurred some mechanical or thermal shock prior to polishing. Comparison with the polished sections of other samples prepared in the same manner (15) and having the same composition failed to confirm this feature as an intrinsic characteristic of

the 5 and 10 mol % materials. Because of the duplex nature of the microstructure of the intermediate compositions and the difficulty in adequately resolving the fine-grained material with an optical microscope, the various compositions were also examined by scanning electron microscopy.

Scanning Electron Microscopy

Samples of each composition were fractured at room temperature, mounted on a specimen holder with a conductive silver paste and coated with ~40 μm (400 Å) of an evaporated carbon layer prior to examination in an SEM. Typical examples of the microstructures are shown in Fig. 31.

The progressive increase in the grain size with increasing amounts of CaO is confirmed. Although not revealed in the optical micrographs, it can be seen that the 5 mol % material also has a duplex structure, albeit with a small amount of the coarse-grained component. On

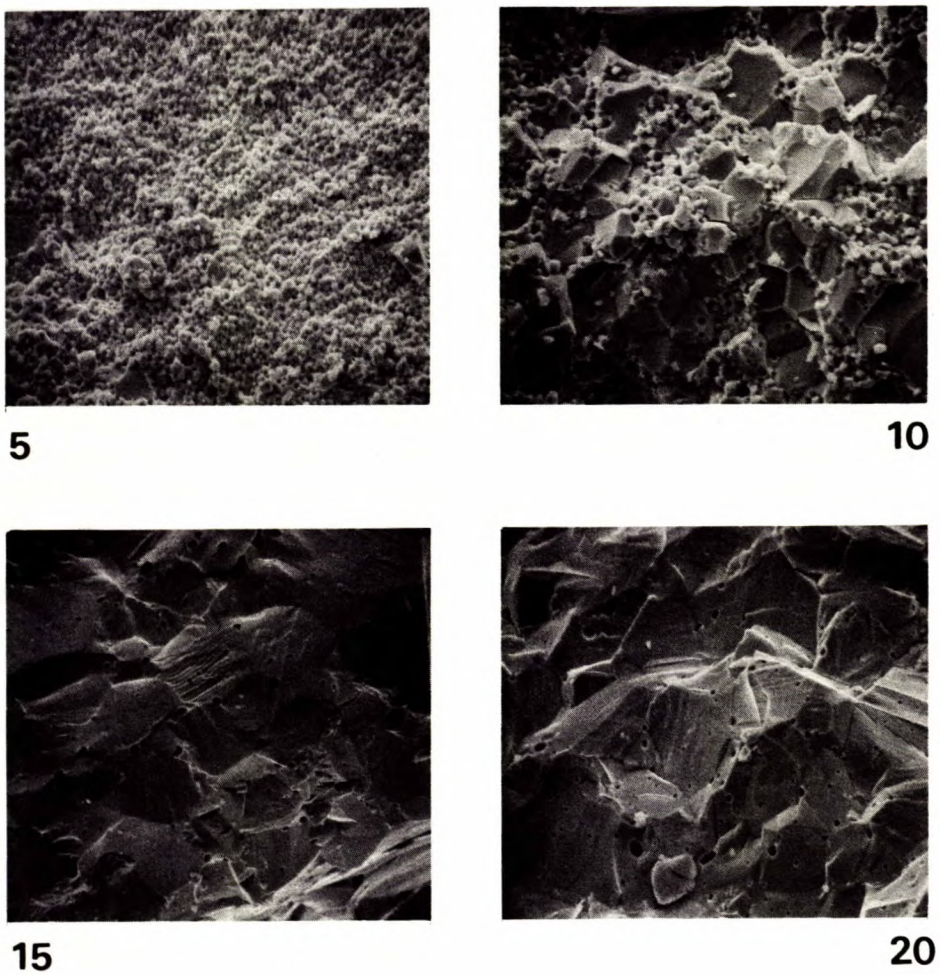

Fig. 31 - SEM micrographs of the fracture surfaces of materials sintered to 1550°C for 6 h. The percentage molar concentration of CaO in each sample is given.

the basis of the smooth transition from the very fine-grained material found in the undoped material to the coarse-grained product developed with 15 mol % CaO, it can be concluded that CaO acts as a grain-growth promoter in sintered ZrO_2.

Comparison of the fracture surfaces of each composition shows that the mode of fracture is completely intergranular up to 10 mol % CaO; at higher concentrations the fracture mode is predominantly transgranular with probably less than 10% being intergranular.

Irrespective of the CaO concentration, the pore size distribution appears to be constant with a mean size of ~1 μm. With the gradual transition from a fine- to a coarse-grained microstructure that occurs with increasing CaO concentrations, it can be seen that the porosity gradually becomes trapped within the grains themselves. This change from entirely intergranular porosity at low CaO concentrations to predominantly intragranular at higher concentrations may be the reason the fracture mode changes from intergranular to transgranular. In turn, this is dictated by the rapid grain growth that occurs as the coarse grains are formed. Under these circumstances, the grain boundaries move too rapidly to allow elimination of the pores located on the boundaries. This gives rise to the microstructures shown in Fig. 31 for the 15 and 20 mol % materials, in which virtually all the porosity is trapped within the grains, hence an end-point density is reached during the sintering cycle. This is why no attempt was made to increase the sintered density to develop theoretically dense samples - no mechanism exists to eliminate the remaining ~4% porosity.

CONCLUSIONS

High reactive, homogeneous CaO-stabilized zirconia powders can readily be prepared using a wet chemical procedure in which freshly precipitated $Zr(OH)_4$ is doped with a calcium formate solution, spray frozen, freeze dried and calcined in air at ~1000°C producing material having a surface area of 20 m^2/g.

By ball milling the calcined powders in methanol containing dissolved polyvinyl acetate and polyethylene glycol, the friable powders can readily be dispersed. Subsequent spray drying of the slurry produces a nearly free-flowing powder that can be isostatically pressed to a relative density of 48% at 210 MPa. By granulating these initially pressed bodies and reducing to minus 200-mesh powder, reforming, and isostatically pressing at 315 MPa, a relatively density of 56% is developed.

All compositions can be readily sintered in air to high density. Using a heating rate of 0.125°C/min in the critical range between 1200 and 1550°C, all compositions were sintered to relative densities between 95 and 98%. Sound sintered discs could be made using any of the doped compositions; only the undoped powder produced badly cracked bodies.

The phase composition of the sintered material was controlled by the amount of stabilizer used. The initially undoped material, which consists of monoclinic zirconia, contains progressively increasing amounts of the cubic phase as the CaO content increases, becoming completely cubic at 10 mol % CaO. This phase is retained between 10 and 20 mol % CaO; at higher concentrations, second phase $CaZrO_3$ is formed.

Coincident with these changes, the grain size increases markedly as the CaO concentration is increased from the partially stabilized region between 0 and 10 mol % CaO to the fully stabilized region between 10 and 20 mol % CaO. It was found that the grain size increases an order of magnitude as the composition changes from the two- to the single-phase region.

Because of the disparity in the expansion coefficients between the cubic and monoclinic phases and especially because of the disruptive phase change that accompanies the monoclinic to tetragonal transition on heating and cooling, the partially stabilized compositions are always formed with considerable stress in the sintered bodies. In some cases, this may lead to severe cracking and warping during either the firing or cooling cycles. Attempts to alleviate this stress by a thermal annealing process are

never successful and only lead to progressive and irreversible expansion.

Although the X-ray diffraction patterns of the sintered solid material gradually change with repeated thermal cycling and approach of the loose powder of the same partially stabilized composition, it is impossible to develop solid sintered bodies having the same stress level found in the powder. For this reason, it can be anticipated that the thermal and electrical properties of the two-phase materials will prove to be strongly dependent on thermal history. This may be of extreme importance in the engineering use of zirconia electrolytes in energy systems such as MHD generators and fuel cells as it is probable that a partially stabilized material would be used to exploit the extremely high thermal-shock resistance that is typical of these compositions. With the repeated thermal cycling that can be expected during use, it is possible that changes in the thermal conductivity and diffusivity and also the electrical properties may impose additional design restrictions.

ACKNOWLEDGEMENTS

The author wishes to express his appreciation to members of the Industrial Minerals Laboratory and other CANMET staff who contributed to this report.

Thanks are particularly due to A.J. Hanson who conducted much of the technical and processing aspects of this work.

REFERENCES

1. Wheat, T.A. "Microstructure of thermal shock resistant zirconia"; J Can Ceram Soc; 44:7-15; 1975.

2. Carter, R.E. and Roth, W.L. "Conductivity and structure in calcia stabilized zirconia"; General Electric Research and Development Center; Research Report 67-C-308; Aug. 1967.

3. Kumar, A. et al. "Effect of oxide defect structure on the electrical properities of zirconia"; J Am Ceram Soc; 55:9:439-445; 1972.

4. Sheindlin, A.E. "Research on MHD power generation in the Soviet Union"; Seminar sponsored by National Research Council; Ottawa, 22 June, 1976.

5. Reed, T.B. and Lerner, R.M. "Methanol: A versatile fuel for immediate use"; Energy: Use Conservation and Supply; 131-136; 1974. Published by AAAS; miscellaneous publication number 74-15.

6. Bockris, J.O'M. " A hydrogen economy"; Science; 176:1323; 1972. Also Gregory, D.P. "The hydrogen economy"; Sci Am; 228:13-21; 1973.

7. Kyle, M.L. et al. Argonne National Lab; Report; ANL 7958; March 1973.

8. Binder, H. et al. "Electrochemische oxydation von Kohlenwasserstoffen in einer Festelectrolytbrennstofzelle bei Temperaturen von 900-1000°C"; [Electrochemical oxidation of hydrocarbons in a solid electrolyte fuel cell at temperatures of 900-1000°C]; Electrochim Acta; 8:781-793; 1963.

9. Schnettler, F.J. et al. "A cryochemical method for preparing ceramic materials"; Sci Ceram; IV:79-90; 1968.

10. McNamara, V.M. "A wet chemical method for preparation of oxide mixtures applicable to electronic ceramics"; J Can Ceram Soc; 34: 103-120; 1965.

11. Mazdiyasni, K.S. "Preparation of high-purity submicron barium titanate powders"; J Am Ceram Soc; 52:523-526; 1969.

12. Carruthers, T.G. and Wheat, T.A. "Hot pressing of kaolin and mixtures of alumina and silica"; Proc Brit Ceram Soc; 3:259-273; 1965.

13. Wheat, T.A. and Mirkovich, V.V. Unpublished data 1970.

14. Wheat, T.A. "Preparation and characterization lime-stabilized zirconia"; J Can Ceram Soc; 42:11-18; 1973

15. Wheat, T.A. "Development of a zirconia electrolyte for use in a steel-making oxygen probe"; CANMET, Energy, Mines and Resources Canada; CANMET Report 76-13; 1976.

16. Thompson, M.A. et al. "Influence of precipitating atmosphere on sintering of ZrO_2 + 12 mol% Y_2O_3"; J Am Ceram Soc; 56:12:648-654; 1974.

17. Pincus, A.G. and Shipley, L.E. "The role of organic binders in ceramic processing"; Ceram Ind; 106-109 & 146; April 1969.

18. Wheat, T.A. "Pilot plant testing of a zirconia-based oxygen probe"; J Can Ceram Soc; 45:5-13; 1976.

19. Garvie, R.C. and Nicholson, P.S. "Structure and thermomechanical properties of partially stabilized zirconia in the $CaO-ZrO_2$ system"; J Am Ceram Soc; 55:3:152-157; 1972.

20. MacDonald, W.A. et al. "A method for the rapid mounting and polishing of ceramic materials for microstructural examinations"; J Mat Sci; 13:905-906; 1978.

21. Porter, D.L. and Heuer, A.H. "Mechanisms of toughening partially stabilized zirconia (PSZ)"; J Am Ceram Soc: 60:3:183-184; 1977.

CANMET REPORTS

Recent CANMET reports presently available or soon to be released through Printing and Publishing, Supply and Services, Canada (addresses on inside front cover), or from CANMET Publications Office, 555 Booth Street, Ottawa, Ontario, K1A 0G1:

Les récents rapports de CANMET, qui sont présentement disponibles ou qui ce seront bientôt peuvent être obtenus de la direction de l'Imprimerie et de l'Edition, Approvisionnements et Services, Canada (adresses au verso de la page couverture), ou du Bureau de Vente et distribution de CANMET, 555 rue Booth, Ottawa, Ontario, K1A 0G1:

78-4 Thermal hydrocracking of Athabasca bitumen: Computer simulation of feed and product vaporization; D.J. Patmore, B.B. Pruden and A.M. Shah;
Cat. no. M38-13/78-4, ISBN 0-660-10021-5; Price: $1.75 Canada, $2.10 other countries.

78-7 Mine dust sampling system - CAMPEDS; G. Knight;
Cat. no. M38-13/78-7, ISBN 0-660-10211-0; Price: $3.50 Canada, $4.20 other countries.

78-12 CANMET review 1977-78; Branch annual report;
Cat. no. M38-13/78-12, ISBN 0-660-10143-2; Price: $2.25 Canada, $2.70 other countries.

78-16 Fly ash for use in concrete part II - A critical review of the effects of fly ash on the properties of concrete; E.E. Berry and V.M. Malhotra;
Cat. no. M38-13/78-16, ISBN 0-660-10129-7; Price: $2.25 Canada, $2.70 other countries.

78-20 Comparison of thermal hydrocracking with thermal cracking of Athabasca bitumen at low conversions; R.B. Logie, R. Ranganathan, B.B. Pruden and J.M. Denis;
Cat. no. M38-13/78-20, ISBN 0-660-10182-3; Price: $1.25 Canada, $1.50 other countries.

78-21 Ceramic clays and shales of the Atlantic Provinces; K.E. Bell, J.G. Brady and L.K. Zengals;
Cat. no. M38-13/78-21, ISBN 0-660-10214-5; Price: $3.00 Canada, $3.60 other countries.

78-22 Radiochemical procedures for determination of selected members of the uranium and thorium series; Edited and compiled by G.L. Smithson;
Cat. no. M38-13/78-22, ISBN 0-660-10081-9; Price: $4.25 Canada, $5.10 other countries.

78-26 Effect of hydrocracking Athabasca bitumen on sulphur-type distribution in the naphtha fraction; A.E. George, B.B. Pruden and H. Sawatzky;
Cat. no. M38-13/78-26, ISBN 0-660-10216-1; Price $1.25 Canada, $1.50 other countries.

78-30 Reduction rates of iron ore-char briquets used in cupola-smelting; J.F. Gransden, J.T. Price and N.J. Ramey;
Cat. no. M38-13/78-30, ISBN 0-660-10215-3; Price: $1.25 Canada, $1.50 other countries.

78-31 Coal associated materials as potential non-bauxite sources of alumina; A.A. Winer and T.E. Tibbetts;
Cat. no. M38-13/78-31, ISBN 0-660-10217-X; Price: $1.25 Canada, $1.50 other countries.